

Spin orbit coupling in bulk ZnO and GaN

J. Y. Fu and M. W. Wu*

*Hefei National Laboratory for Physical Sciences at Microscale,
University of Science and Technology of China, Hefei, Anhui, 230026, China and*

*Department of Physics, University of Science and Technology of China, Hefei, Anhui, 230026, China
(Dated: September 20, 2008)*

Using group theory and Kane-like $\mathbf{k} \cdot \mathbf{p}$ model together with the Löwdining partition method, we derive the expressions of spin-orbit coupling of electrons and holes, including the linear- k Rashba term due to the intrinsic structure inversion asymmetry and the cubic- k Dresselhaus term due to the bulk inversion asymmetry in wurtzite semiconductors. The coefficients of the electron and hole Dresselhaus terms of ZnO and GaN in wurtzite structure and GaN in zinc-blende structure are calculated using the nearest-neighbor sp^3 and sp^3s^* tight-binding models separately.

PACS numbers: 71.70.Ej, 85.75.-d, 72.80.Ey

I. INTRODUCTION

The wide gap semiconductors ZnO, GaN and their alloys with wurtzite or zinc-blende structures have provoked a lot of interest in the last few years, largely due to the good optical properties as well as great potential in optoelectronics.^{1,2,3,4} Very recently, some attention has also been given to the spin properties of these semiconductors.^{5,6,7,8,9} This is partly because of the prediction that ZnO can become ferromagnetic with a Curie temperature above room temperature if doped with manganese.¹⁰ Ferromagnetism and magnetoresistance in Co-ZnO magnetic semiconductors have been also reported.⁷ Moreover, long spin relaxation time observed in these materials is another promising property for possible applications in spintronic devices. Ghosh *et al.*⁸ have investigated the electron spin properties in n -type ZnO structures and discovered the electron spin relaxation time varying from 20 ns to 190 ps when the temperature increases from 10 to 280 K. Room temperature electron spin relaxation as long as 25 ns has also been measured by electron paramagnetic resonance spectroscopy in colloidal n -doped ZnO quantum dots.⁹ In GaN, Beschoten *et al.*¹¹ reported the electron spin lifetime of 20 ns from $T = 5$ K to room temperature. Recently, hole spin relaxation time about 350 ps at 1.7 K in ZnO epilayer has also been reported.¹²

Spin-orbit coupling (SOC) is the key issue of semiconductor spintronics.^{13,14} Most of the proposed schemes of electrical generation, manipulation and detection of electron or hole spins rely on the SOC. A thorough understanding of the SOC is therefore very important. In contrast to the zinc-blende semiconductors such as GaAs, the existence of hexagonal c axis in wurtzite semiconductors leads to an added intrinsic wurtzite structure inversion asymmetry (WSIA) in addition to the bulk inversion asymmetry (BIA).^{15,16} Therefore, the electron spin splittings include both the Dresselhaus effect (cubic in k) and Rashba effect (linear in k).^{17,18} The Rashba effect has been vigorously discussed using group theory and $\mathbf{k} \cdot \mathbf{p}$

arguments by Lew Yan Voon *et al.*¹⁹ It was pointed out that the Rashba SOC coefficient is very small (about 1.1 meV·Å) in ZnO.¹⁹ Majewski and Vogl reported a value of 9 meV·Å of the Rashba coefficient in GaN based on the first principle calculation.²⁰ Magneto-transport measurements in GaN heterostructure gave the Rashba coefficient ranging from 5.5 to 10.01 meV·Å.^{21,22,23,24} For electron Dresselhaus effect in wurtzite semiconductors, Wang *et al.* gave the form of electron Dresselhaus SOC $H_{so} = \gamma_e(bk_z^2 - k_{\parallel}^2)(\sigma_x k_y - \sigma_y k_x)$ recently with γ_e and b the SOC parameters. By fitting a spin degenerate surface near the Γ point, they obtained $b = 4.028$ and $\gamma_e \sim 0.74$ meV·Å³ for AlN.²⁵ However, up to now, there is no report on the Dresselhaus coefficients in ZnO and GaN. Additionally, there is no investigation on the SOC in valence bands.

In this work, by using group theory and $\mathbf{k} \cdot \mathbf{p}$ method, we first construct the 8×8 Kane model for wurtzite structure, including the s - p_z mixing of the lowest conduction band as well as the contributions from the remote bands. Then we derive the forms of the SOC for both electron and hole by Löwdining partition method.²⁶ The electron and hole Dresselhaus SOC coefficients in wurtzite ZnO and GaN are then investigated in detail by using the sp^3 nearest-neighbor tight-binding (TB) model, which was first put forward for wurtzite semiconductors by Kobayashi *et al.*,²⁷ however, without the SOC effect. We incorporate the SOC following the approach by Chadi.²⁸

This paper is organized as follows: In Sec. II, we present the model. We start with the Kane-like $\mathbf{k} \cdot \mathbf{p}$ model for wurtzite semiconductors and derive the expressions for the SOC for electron and hole perturbatively up to third order in Sec. IIA. In Sec. IIB, we briefly introduce the nearest-neighbor sp^3 TB model for wurtzite semiconductors. We present our main results in Sec. III and conclude in Sec. IV.

II. MODEL AND HAMILTONIAN

In contrast to the form given by Chuang and Chang,²⁹ in which the s - p_z mixing of the lowest conduction band and the contributions from the remote bands are missing, in this section, we first construct the 8×8 Kane-like $\mathbf{k} \cdot \mathbf{p}$ model for wurtzite semiconductors with the s - p_z mixing properly included. The contributions from the remote bands are also considered perturbatively. Then we derive the expressions of SOC for both electron and hole. Finally, we briefly introduce the sp^3 TB model for the wurtzite semiconductors which we use for obtaining the SOC coefficients.

A. Kane-like $\mathbf{k} \cdot \mathbf{p}$ model

The Schrödinger equation relating the periodic part $u_{\nu\mathbf{k}}(\mathbf{r})$ of the Bloch function and the energy near the band edge has the form^{30,31}

$$\begin{aligned} H u_{\nu\mathbf{k}}(\mathbf{r}) &\approx (H_0 + \frac{\hbar^2 k^2}{2m_0} + \frac{\hbar}{m_0} \mathbf{k} \cdot \mathbf{p} + H_{so}) u_{\nu\mathbf{k}}(\mathbf{r}) \\ &= E_n(\mathbf{k}) u_{\nu\mathbf{k}}(\mathbf{r}), \end{aligned} \quad (1)$$

where

$$H_0 = \frac{p^2}{2m_0} + V(\mathbf{r}), \quad (2)$$

$$\begin{aligned} H_{so} &= \frac{\hbar}{4m_0^2 c^2} \nabla V \times \mathbf{p} \cdot \boldsymbol{\sigma} \\ &= H_{sx} \sigma_x + H_{sy} \sigma_y + H_{sz} \sigma_z. \end{aligned} \quad (3)$$

Here $V(\mathbf{r})$ is the periodic potential, H_{so} accounts for the spin-orbit interaction, and σ_i with $i = x, y, z$ are the Pauli spin matrices.

Following Chuang and Chang, the basis functions used near the zone center read $|u_1\rangle = |iS \uparrow\rangle$, $|u_2\rangle = \left| -\frac{X+iY}{\sqrt{2}} \uparrow \right\rangle$, $|u_3\rangle = \left| \frac{X-iY}{\sqrt{2}} \uparrow \right\rangle$, $|u_4\rangle = |Z \uparrow\rangle$, $|u_5\rangle = |iS \downarrow\rangle$, $|u_6\rangle = \left| \frac{X-iY}{\sqrt{2}} \downarrow \right\rangle$, $|u_7\rangle = \left| -\frac{X+iY}{\sqrt{2}} \downarrow \right\rangle$, and $|u_8\rangle = |Z \downarrow\rangle$.²⁹ Here $|S\rangle$, $|X\rangle$, $|Y\rangle$, and $|Z\rangle$ represent the symmetry of the band edge states, and the arrows stand for the spin orientation. The z direction corresponds to the c axis of the wurtzite crystal. From the C_{6v} symmetry analysis of point group for the wurtzite structure, the $\mathbf{k} \cdot \mathbf{p}$ Hamiltonian in the basis of $|u_i\rangle$ with $i = 1, \dots, 8$ can be written as

$$H_{8 \times 8} = \frac{\hbar^2 k^2}{2m_0} + \begin{pmatrix} E_c + \frac{\hbar^2 k^2}{2m'} & -\frac{P_2}{\sqrt{2}} k_+ - iB_{cv1} k_z k_+ & \frac{P_2}{\sqrt{2}} k_- & P_1 k_z - iB_{cv2} k_{\parallel}^2 & 0 & 0 & -\sqrt{2}i\Delta_{sz} & 0 \\ -\frac{P_2}{\sqrt{2}} k_- + iB_{cv1} k_z k_- & E_v + \Delta_1 + \Delta_2 + A' k_z^2 & 0 & \frac{iQ}{\sqrt{2}} k_- + B_{cv3} k_z k_- & 0 & 0 & 0 & 0 \\ \frac{P_2}{\sqrt{2}} k_+ & 0 & E_v + \Delta_1 - \Delta_2 & -\frac{iQ}{\sqrt{2}} k_+ & \sqrt{2}i\Delta_{sz} & 0 & 0 & \sqrt{2}\Delta_3 \\ P_1 k_z + iB_{cv2} k_{\parallel}^2 & -\frac{iQ}{\sqrt{2}} k_+ + B_{cv3} k_z k_+ & \frac{iQ}{\sqrt{2}} k_- & E_v + B' k_{\parallel}^2 & 0 & 0 & \sqrt{2}\Delta_3 & 0 \\ \frac{P_2}{\sqrt{2}} k_+ & 0 & -\sqrt{2}i\Delta_{sz} & 0 & E_c + \frac{\hbar^2 k^2}{2m'} & \frac{P_2}{\sqrt{2}} k_- + iB_{cv1} k_z k_- & -\frac{P_2}{\sqrt{2}} k_+ & P_1 k_z - iB_{cv2} k_{\parallel}^2 \\ 0 & 0 & 0 & 0 & \frac{P_2}{\sqrt{2}} k_- + iB_{cv1} k_z k_+ & E_v + \Delta_1 + \Delta_2 + A' k_z^2 & 0 & -\frac{iQ}{\sqrt{2}} k_+ - B_{cv3} k_z k_+ \\ \sqrt{2}i\Delta_{sz} & 0 & 0 & \sqrt{2}\Delta_3 & -\frac{P_2}{\sqrt{2}} k_- & 0 & E_v + \Delta_1 - \Delta_2 & \frac{iQ}{\sqrt{2}} k_- \\ 0 & 0 & \sqrt{2}\Delta_3 & 0 & P_1 k_z + iB_{cv2} k_{\parallel}^2 & \frac{iQ}{\sqrt{2}} k_- - B_{cv3} k_z k_- & -\frac{iQ}{\sqrt{2}} k_+ & E_v + B' k_{\parallel}^2 \end{pmatrix}, \quad (4)$$

in which $k_{\pm} = k_x \pm ik_y$. The energy parameters are defined by $\langle S|H_0|S\rangle = E_c$, $\langle X|H_0|X\rangle = \langle Y|H_0|Y\rangle = E_v + \Delta_1$, $\langle Z|H_0|Z\rangle = E_v$, $\langle Y|H_{sz}|X\rangle = i\Delta_2$, and $\langle Z|H_{sx}|Y\rangle = -\langle Z|H_{sy}|X\rangle = i\Delta_3$. The interband momentum-matrix elements read $P_1 = -\frac{i\hbar}{m_0} \langle S|p_z|Z\rangle$, $P_2 = -\frac{i\hbar}{m_0} \langle S|p_x|X\rangle = -\frac{i\hbar}{m_0} \langle S|p_y|Y\rangle$, and $Q = -\frac{i\hbar}{m_0} \langle Z|p_x|X\rangle = -\frac{i\hbar}{m_0} \langle Z|p_y|Y\rangle$. It is noted that the parameter Q was omitted in Ref. 29. The inclusion of Q gives an improved description of the valence bands. It

also determines the hole spin splitting.³² The other parameters m' , B_{cv1} , B_{cv2} , B_{cv3} , A' , and B' are related with the contributions from the remote bands, which were also omitted in Ref. 29. Δ_{sz} originates from the s - p_z mixing of the lowest conduction band and has the same definition as the energy parameter Δ_3 . In addition, Δ_{sz} is closely related to the linear Rashba terms of both electron and hole.^{19,33} This term was also omitted in Ref. 29. As for the energy parameters Δ_1 , Δ_2 and Δ_3 , one

can relate them to crystal-field split energy Δ_{cr} and the spin-orbit split-off energy Δ_{so} by

$$\Delta_1 = \Delta_{cr}, \quad \Delta_2 = \Delta_3 = \frac{1}{3}\Delta_{so}. \quad (5)$$

Using Löwdin partition method,²⁶ one can derive the SOC terms for electron and hole, which act as k -dependent effective magnetic fields. For the states near Γ point, the electron SOC can be described by $[\alpha_e \mathbf{\Omega}_e^R(\mathbf{k}) + \gamma_e \mathbf{\Omega}_e^D(\mathbf{k})] \cdot \boldsymbol{\sigma}$ with

$$\alpha_e \mathbf{\Omega}_e^R(\mathbf{k}) = \alpha_e(k_y, -k_x, 0), \quad (6)$$

$$\gamma_e \mathbf{\Omega}_e^D(\mathbf{k}) = \gamma_e(bk_z^2 - k_{\parallel}^2)(k_y, -k_x, 0). \quad (7)$$

Here $\alpha_e \mathbf{\Omega}_e^R(\mathbf{k})$ and $\gamma_e \mathbf{\Omega}_e^D(\mathbf{k})$ are the Rashba and Dresselhaus terms, respectively. α_e and γ_e are the corresponding SOC coefficients. b is a parameter that can be determined by the TB calculation. It should be mentioned that α_e originates from the s - p_z mixing of the lowest conduction band, whereas γ_e is closely related with $\mathbf{k} \cdot \mathbf{p}$ interaction with the remote bands having Γ_6 symmetry.

As we know, for zinc-blende structure, both the heavy hole (HH) and light hole (LH) belong to the four dimensional Γ_{8v} group presentation whereas the spin split-off hole (SOH) has the Γ_{7v} symmetry.^{31,34} However, for wurtzite structure, the combination of crystal-field and SOC energies lead to a three-edge structure at the top of the valence band. Two of these three edges are of Γ_{7v} symmetry and the remaining one is of Γ_{9v} symmetry. The symmetry of the valence bands are, in the order of decreasing energy, Γ_{9v} (HH), Γ_{7v} (LH), and $\Gamma_{7'v}$ (crystal-field split-off hole) for GaN^{35,36} and Γ_{7v} (HH), Γ_{9v} (LH), and $\Gamma_{7'v}$ (crystal-field split-off hole) for ZnO.^{19,37} This anomalous ordering in ZnO results from a negative spin-orbit splitting.³⁸ Hereafter, in the description of the SOC of holes of ZnO and GaN, we use the subscript “9”, “7”, and “7'” from the symmetry representation to label the three kinds of holes above. For the lowest conduction band, both ZnO and GaN have Γ_{7c} symmetry and we use the symbol “e” to denote it. The corresponding SOC terms are $[\alpha_i \mathbf{\Omega}_i^R(\mathbf{k}) + \gamma_i \mathbf{\Omega}_i^D(\mathbf{k})] \cdot \boldsymbol{\sigma}$, which include both the linear Rashba term $\alpha_i \mathbf{\Omega}_i^R(\mathbf{k})$, and the cubic Dresselhaus term $\gamma_i \mathbf{\Omega}_i^D(\mathbf{k})$, with $i = e, 9, 7, 7'$. Their expressions are given in Table I.

The Rashba coefficients α_i with $i = e, 7, 7'$ are expressed using the $\mathbf{k} \cdot \mathbf{p}$ parameters:

$$\alpha_e = \frac{2P_2\Delta_{sz}}{E_g + \Delta_{so}}, \quad (8)$$

$$\alpha_7 = 2\left(\frac{Q\Delta_{so}}{3\Delta_{cr}} - \frac{P_2\Delta_{sz}}{E_g + \Delta_{so}}\right), \quad (9)$$

$$\alpha_{7'} = \frac{-2Q\Delta_{so}}{3\Delta_{cr}}, \quad (10)$$

where E_g is the energy gap between the bottom of the conduction band and the top of the valence band. As for Γ_{9v} symmetry, there is no linear- k splitting, namely the Rashba coefficient $\alpha_9 = 0$, as pointed out in previous

literature.^{39,40} Moreover, it is noted for the expression of α_7 [Eq. (9)] that the first term dominates due to the large band gap in ZnO and GaN. Therefore, due to the negative spin splitting energy in ZnO, both α_e and α_7 are negative. However, they are positive for GaN. The situation of $\alpha_{7'}$ is reversed.

As for the Dresselhaus effect, both the SOC coefficient γ_i and the parameter b can be determined by the TB calculation. While it should be mentioned that γ_i is closely related with the remote bands with Γ_6 symmetry. It is also noted that the electron Rashba and Dresselhaus terms of ZnO and GaN have opposite signs. However, it is not the case for Γ_{7v} and $\Gamma_{7'v}$ holes. For the Γ_{9v} holes, only the Dresselhaus term exists.

For the sake of comparison, SOC terms of zinc-blende structures³¹ are also listed in Table I. For Γ_{8v} valence band, the SOC form reads $\gamma_8 \mathbf{\Omega}_8^D \cdot \mathbf{J}$. Here the small modifications from the $\mathbf{k} \cdot \mathbf{p}$ interactions with the remote Γ_3 state and the SOC within the conduction band Γ_{8c} are omitted. The matrices J_i with $i = x, y, z$ are angular momentum matrices for angular momentum $J = 3/2$.

B. TB model

To calculate electron and hole spin splittings, we use the sp^3 TB model elaborated by Kobayashi *et al.*,²⁷ which has been proven to be an effective approach in band structure calculations for wurtzite crystals.^{27,41,42} In this model, the local point symmetry is approximately tetrahedral, namely T_d symmetry rather than C_{3v} symmetry. In such an approximation, on-site coupling between s and p_z orbitals, and the small crystal field splittings between p_z orbital and the $p_{x,y}$ orbital are both neglected. Thus the model has nine independent parameters: the four on-site matrix elements $E(s, a)$, $E(p, a)$, $E(s, c)$, $E(p, c)$ (where s and p refer to the basis states, and a and c refer to anion and cation), and five transfer matrix elements $V(ss\sigma)$, $V(sp\sigma)$, $V(ps\sigma)$, $V(pp\pi)$, and $V(pp\sigma)$ [where the orientation of the p orbitals is denoted by σ and π , and the first (second) index refers to the s or p state of anion (cation)]. For numerical calculations, we use the TB parameters taken from Refs. 27 and 41.

The SOC is included as outlined by Chadi.²⁸ We take the spin splitting parameters $\Delta_{zn}=0.335$ eV, $\Delta_o=0.0274$ eV, $\Delta_{Ga}=0.174$ eV, and $\Delta_N=0.009$ eV.^{28,43,44} It should be mentioned that only the cubic term, namely the Dresselhaus spin splitting can be calculated by the TB model under T_d symmetry approximation. Based on the zero spin splitting point calculated by the TB model, one can conveniently fit the parameter b in the Dresselhaus SOC descriptions listed in Table I. Moreover, the SOC coefficient γ_i can also be obtained from the calculated spin splitting energy.

TABLE I: Electron and hole SOC terms. $\alpha_i\Omega_i^R(\mathbf{k})$ and $\gamma_i\Omega_i^D(\mathbf{k})$ represent the Rashba and Dresselhaus terms with $i = e, 9, 7, 7'$ for wurtzite structure and $i = e, 8, 7$ for zinc-blende structure. α_i and γ_i are the Rashba and Dresselhaus SOC coefficients.

1. Wurtzite structure	$\alpha_i\Omega_i^R(\mathbf{k})$	$\gamma_i\Omega_i^D(\mathbf{k})$
Conduction band (Γ_{7c}):	$\alpha_e(k_y, -k_x, 0)$	$\gamma_e(bk_z^2 - k_{\parallel}^2)(k_y, -k_x, 0)$
(Γ_{9v}):	0	$\gamma_9(k_y(k_y^2 - 3k_x^2), k_x(k_x^2 - 3k_y^2), 0)$
Valence bands (Γ_{7v}):	$\alpha_7(k_y, -k_x, 0)$	$\gamma_7(bk_z^2 - k_{\parallel}^2)(k_y, -k_x, 0)$
($\Gamma_{7'v}$):	$\alpha_{7'}(k_y, -k_x, 0)$	$\gamma_{7'}(bk_z^2 - k_{\parallel}^2)(k_y, -k_x, 0)$
2. Zinc-blende structure ³¹	$\alpha_i\Omega_i^R(\mathbf{k})$	$\gamma_i\Omega_i^D(\mathbf{k})$
Conduction band (Γ_{6c}):	0	$\gamma_e(k_x(k_y^2 - k_z^2), k_y(k_z^2 - k_x^2), k_z(k_x^2 - k_y^2))$
Valence bands (Γ_{8v}):	0	$\gamma_8(k_x(k_y^2 - k_z^2), k_y(k_z^2 - k_x^2), k_z(k_x^2 - k_y^2))$
(Γ_{7v}):	0	$\gamma_7(k_x(k_y^2 - k_z^2), k_y(k_z^2 - k_x^2), k_z(k_x^2 - k_y^2))$

III. RESULTS

Since the linear Rashba term has been investigated in Ref. 19, in this section we mainly discuss the cubic Dresselhaus terms of wurtzite ZnO and GaN, calculated from the nearest-neighbor sp^3 TB model. In fact, the electron Dresselhaus term becomes the dominant SOC compared with the linear Rashba term when the electron concentration is higher than 10^{19} cm^{-3} for ZnO and 10^{20} cm^{-3} for GaN. (Note in the literature, the electron concentrations of ZnO and GaN are in the range of 10^{17} cm^{-3} to 10^{21} cm^{-3} .^{8,24,45}) In order to compare with the zinc-blende structure, the cubic case of GaN is also addressed.

A. SOC in ZnO

In Fig. 1(a), we show the cubic electron spin splitting energy around Γ point for different momentum in the planes of $k_z=0$ (red thin curves), 0.1 \AA^{-1} (blue curves), and 0.15 \AA^{-1} (green thick curves), respectively. In each k_z plane, the results along Γ - K (solid curves) and Γ - M (dashed curves) directions are shown separately. In contrast to the spin splitting of GaAs at Γ point,⁴⁶ one can see from the figure that, for small momentum, the splittings show isotropy. Moreover, in the case of $k_z=0.1 \text{ \AA}^{-1}$, there is a zero splitting point at $k_{\parallel}=0.198 \text{ \AA}^{-1}$, from which one can determine that b in the Dresselhaus term is 3.910. Furthermore, we find from our calculation that there is a certain variation of b as shown in the inset of Fig. 1(a). From the inset one notices that b increases monotonically with k_{\parallel} . It also implies that for small momentum, b keeps constant around 3.855. Moreover, it is independent on the angle of the in-plane wave vector k_{\parallel} , which can be seen from the fact of the same zero splitting points between Γ - K and Γ - M directions under the same wave vector k_z .

Up till now, there has been no report on the value of γ_e . In this work, the value of this coefficient is extracted

from

$$\gamma_e(\mathbf{k}) = \Delta E / (2|\Omega_e^D(\mathbf{k})|), \quad (11)$$

with ΔE standing for the corresponding Dresselhaus spin splitting energy. The results for different momentum are shown in Fig. 1(b-d). One can see from the figure that for small momentum, γ_e is almost a constant (about $0.33 \text{ eV}\cdot\text{\AA}^3$) with its value being almost two orders of magnitude smaller than the electron Dresselhaus coefficient $17.0 \text{ eV}\cdot\text{\AA}^3$ in GaAs,⁴⁶ thanks to the large band gap ($E_g \sim 3.3 \text{ eV}$ at 300 K) in ZnO.⁴⁷ When the momentum lies far away from the Γ point, our calculation indicates that the value of γ_e decreases, either with the increase of the in-plane wave vector k_{\parallel} in Fig. 1(b), or with the out-of-plane wave vector k_z in Fig. 1(c). This k -dependence of γ_e is due to the correction of the higher order SOC terms for large momentum. Moreover, angle dependence of γ_e becomes remarkable for large momentum, which is also because of the correction of higher order SOC terms.

In order to verify the accuracy of our computation, we compare our results with the *ab initio* calculations based on atomic sphere approximation linear-muffin-tin-orbital (ASA-LMTO) method, as shown in Fig. 2. In the figure, the Dresselhaus splitting is from our computation and the Rashba splitting is calculated by using the Rashba coefficient extracted from ASA-LMTO calculations by Lew Yan Voon *et al.*¹⁹ From Fig. 2, one can see that the sum of these two terms is in very good agreement with the ASA-LMTO results, which confirms the soundness of our Dresselhaus spin splitting calculations. This agreement also confirms that the Rashba and Dresselhaus coefficients of electrons have opposite signs.

We now turn to the case of hole SOC. The spin splittings for holes with Γ_{9v} , Γ_{7v} , and $\Gamma_{7'v}$ symmetries are plotted against in-plane momentum in Fig. 3(a) and (b) in the planes of $k_z = 0$ and 0.04 \AA^{-1} respectively. One finds from Fig. 3(a) that as $k_{\parallel} < 0.3 \text{ \AA}^{-1}$, the spin splittings for the holes with Γ_{7v} and $\Gamma_{7'v}$ symmetry increase drastically and become much larger than that of the holes with Γ_{9v} symmetry. The corresponding SOC coefficients γ_i , with $i = 9, 7, 7'$ are also calculated similar to the case

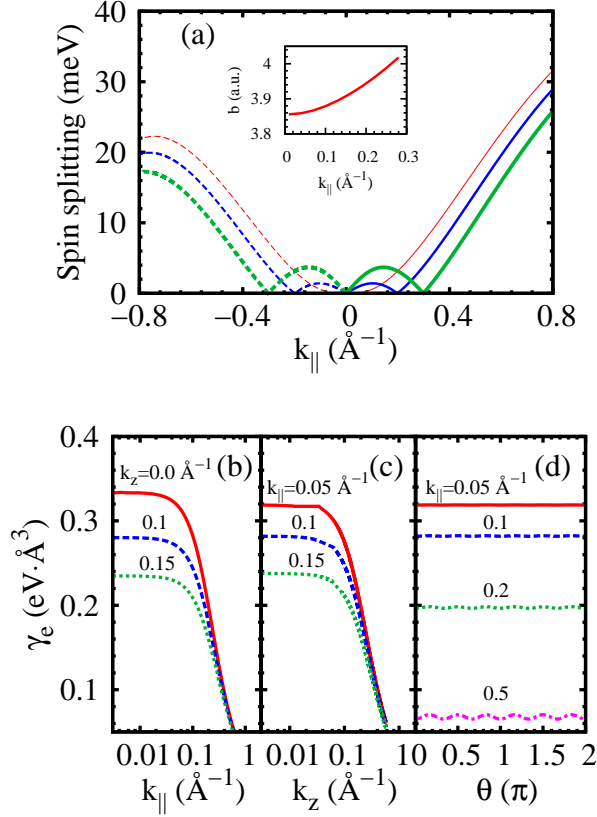


FIG. 1: (Color Online) (a) Electron spin splitting of ZnO against in-plane momentum along Γ - K (solid curves) and Γ - M (dashed curves) directions. Red (thin) curves: $k_z=0$; Blue curves: $k_z=0.1 \text{ \AA}^{-1}$; Green (thick) curves: $k_z=0.15 \text{ \AA}^{-1}$. Inset: The coefficient b as function of $k_{||}$. (b) γ_e vs. $k_{||}$ along Γ - K direction under different k_z . (c) γ_e vs. k_z under different $k_{||}$. (d) γ_e vs. angle of the in-plane momentum at different $k_{||}$ in the plane of $k_z = 0$.

of γ_e . The results are shown in Fig. 3(c-e). Again these coefficients are constants close to the Γ point, where γ_7 and $\gamma_{7'}$ are close to each other, i.e., $\gamma_7 = 6.3 \text{ eV}\cdot\text{\AA}^3$ and $\gamma_{7'} = 6.1 \text{ eV}\cdot\text{\AA}^3$. While for the hole with Γ_{9v} symmetry, the coefficient γ_9 is only about $0.09 \text{ eV}\cdot\text{\AA}^3$. Moreover, γ_i are also angle-independent for small momentum, but become markedly angle-dependent for large momentum. The corresponding results are shown in Fig. 3(d) and (e). Additionally, from the zero spin splitting point in Fig. 3(b) for the holes with Γ_{7v} and $\Gamma_{7'v}$ symmetries (around 0.098 \AA^{-1} in the figure), the parameter b can also be extracted. We obtain almost the identical value as that obtained from the electron SOC under the same momentum.

B. SOC in GaN

GaN shares the same electronic wurtzite structure with ZnO, and also has a direct wide gap about 3.4 eV .⁴⁸ In

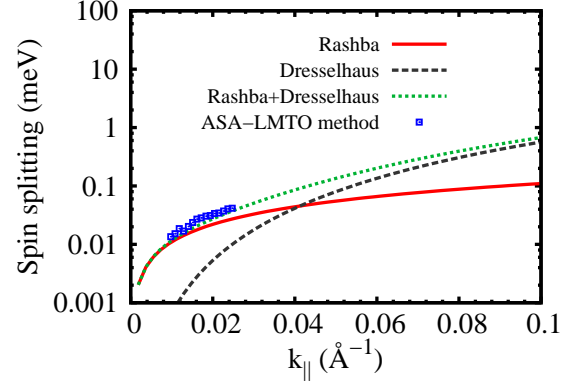


FIG. 2: (Color Online) Electron spin splitting in ZnO against momentum along Γ - K direction. The splitting from the Rashba term and from the ASA-LMTO calculation are taken from Ref. 19.

TABLE II: Rashba (α_i) (in $\text{meV}\cdot\text{\AA}$) and Dresselhaus (γ_i) (in $\text{eV}\cdot\text{\AA}^3$) SOC coefficients in wurtzite ZnO and GaN at small momentum with $i = e, 9, 7, 7'$.

	α_e	α_9	α_7	$\alpha_{7'}$	γ_e	γ_9	γ_7	$\gamma_{7'}$
ZnO:	1.1 ^a	—	35 ^a (21 ^b)	51 ^a	0.33	0.09	6.3	6.1
GaN:	9.0 ^b	—	45 ^b	32 ^b	0.32	0.07	15.3	15.0

^a from Ref. 19;

^b from Ref. 20

Fig. 4(a), we show the electron Dresselhaus spin splittings around Γ point for different momentums in the planes of $k_z=0$ (red thin curves), 0.1 (blue curves), and 0.15 \AA^{-1} (green thick curves), respectively. One can see from the figure that the momentum dependence of the Dresselhaus splitting is very similar to that in ZnO. In GaN, the Rashba coefficient is also small (about $9 \text{ meV}\cdot\text{\AA}$). We can also estimate that, the Dresselhaus effect becomes dominant when the electron concentration is larger than 10^{20} cm^{-3} . From the point of zero spin splitting, one can calculate b in the Dresselhaus term. The results are shown in the inset of Fig. 4(a). For small momentum, one finds $b \sim 3.959$ in GaN and 3.855 previously in ZnO, both are different but close to 4.028 —the “universal” value for all the wurtzite materials predicted by Wang *et al.* from their AlN investigation.²⁵ Moreover, with the increase of the momentum, similar to the case of ZnO, b can not be regarded as a constant and shows marked k -dependence. In addition, it should be mentioned that, for large momentum, the universality of b for all the wurtzite materials does not hold and this difference enhances with the increase of momentum. For example, when $k_{||} = 0.3 \text{ \AA}^{-1}$, the values for ZnO and GaN are 4.039 and 4.326 , respectively.

For the hole spin splitting, one also obtains the similar results as those of ZnO, as shown in Fig. 4(b) and (c). From Fig. 4, it is implied that both the electron and hole

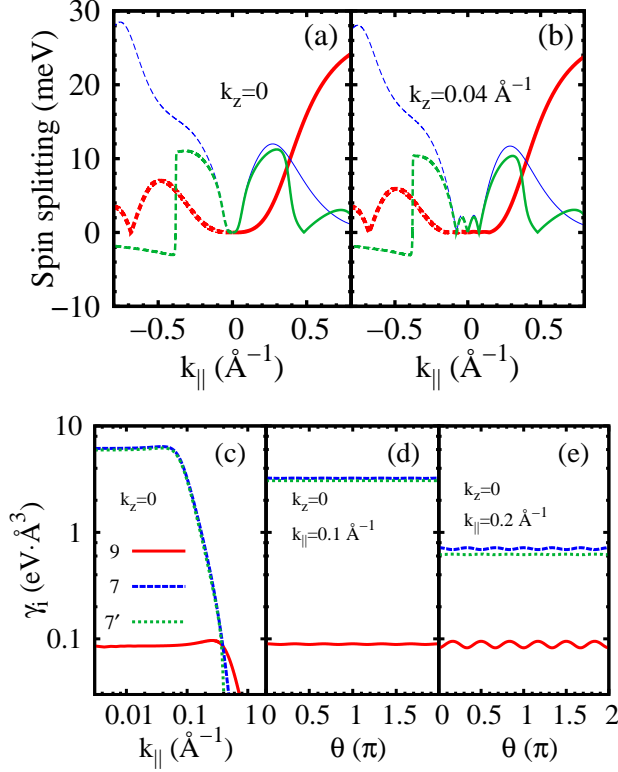


FIG. 3: (Color Online) (a-b) Hole spin splitting in ZnO against momentum along Γ -K (solid curves) and Γ -M (dashed curves) directions with $k_z=0$ in (a) and $k_z=0.04 \text{ \AA}^{-1}$ in (b). (c) Hole SOC coefficients γ_i ($i = 9, 7, 7'$) vs. $k_{||}$ along Γ -K direction; (d-e) γ_i vs. angle of the momentum in the plane of $k_z=0$. $k_{||}=0.1 \text{ \AA}^{-1}$ in (d) and $k_{||}=0.2 \text{ \AA}^{-1}$ in (e). Red curves [thick curves in (a) and (b)]: Γ_{9v} ; Blue curves [thin curves in (a) and (b)]: Γ_{7v} ; Green curves: $\Gamma_{7'v}$.

spin splittings are isotropic at small momentum. The corresponding SOC coefficients γ_i with $i = e, 9, 7, 7'$ as functions of in-plane momentum are shown in Fig. 5(a) with $k_z = 0$. We find γ_e and γ_9 are about 0.32 and $0.07 \text{ eV}\cdot\text{\AA}^3$ for small momentum, respectively. These values are very close to the case of ZnO, which we believe are due to their similar electronic structures and almost equal band gaps. However, as for γ_7 and $\gamma_{7'}$, they are about 15.3 and $15.0 \text{ eV}\cdot\text{\AA}^3$ separately, two times larger than those in ZnO. Similarly, γ_7 and $\gamma_{7'}$ are close to each other. In addition, as the momentum increases, the dependence of the SOC coefficients on the angle of the in-plane-momentum becomes more and more pronounced, as shown in Fig. 5(b-d). The Rashba (α_i) and Dresselhaus (γ_i) SOC coefficients in wurtzite ZnO and GaN for small momentum are summarized in Table II.

In order to have a comparison with the case of zinc-blende structures, we also calculate the spin splitting energy in cubic GaN using sp^3s^* TB model based on the parameters by Reilly *et al.*,⁴⁹ which has proven its capability in the Γ valley band structure calculations.⁴⁶ Both the electron and hole SOC at the Γ point in zinc-blende

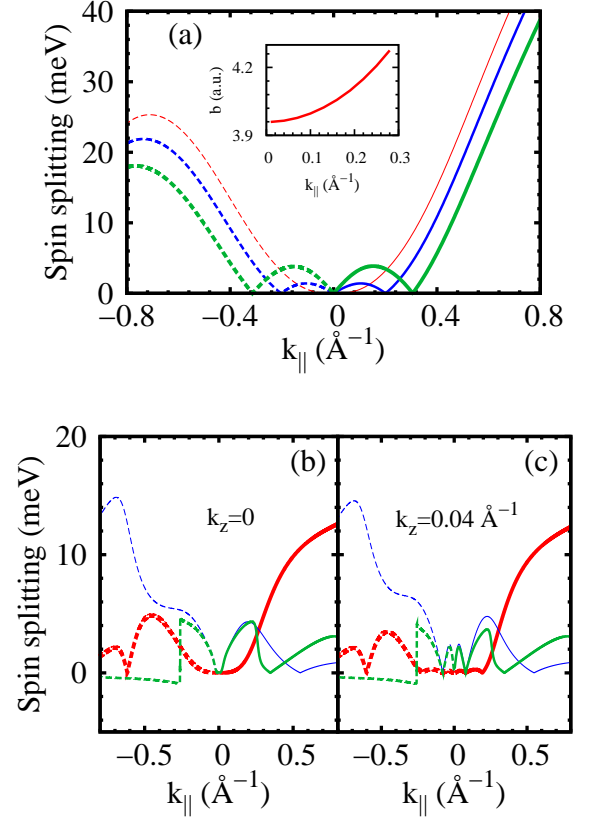


FIG. 4: (Color Online) (a) Electron spin splitting in wurtzite GaN against momentum along Γ -K (solid curves) and Γ -M (dashed curves) directions. Red (thin) curves: $k_z=0$; Blue curves: $k_z=0.1 \text{ \AA}^{-1}$; Green (thick) curves: $k_z=0.15 \text{ \AA}^{-1}$. Inset: The coefficient b as function of $k_{||}$. (b-c) Hole spin splitting in wurtzite GaN against momentum along Γ -K (solid curves) and Γ -M (dashed curves) directions with $k_z=0$ in (b) and $k_z=0.04 \text{ \AA}^{-1}$ in (c). Red (thick) curves: Γ_{9v} ; Blue (thin) curves: Γ_{7v} ; Green curves: $\Gamma_{7'v}$.

crystals have been extensively discussed in Ref. 31 and it is known that only the Dresselhaus term exists in this structure.

The numerical results are shown in Fig. 6. Two typical directions (along Γ -K and Γ -W) of spin splittings for electron and hole are shown in Fig. 6(a). It is implied that even though for small momentum, the spin splittings also show anisotropy. This is not in the case of wurtzite structure. Moreover, the anisotropic spin splitting is more distinct for the HH, as shown in Fig. 6(a). Of course, for large momentum, the spin splittings of both structures show anisotropy. In addition, it is interesting to see that although the lowest conduction band and the SOH band have different symmetries (Γ_{6c} and Γ_{7v} respectively), they share the same form of SOC. From the red and black curves in Fig. 6(a), one can see that electron and SOH have similar momentum dependence of spin splitting.

The electron SOC coefficient is shown in Fig. 6(b) and (c). Similar to the wurtzite case, γ_e keeps constant near

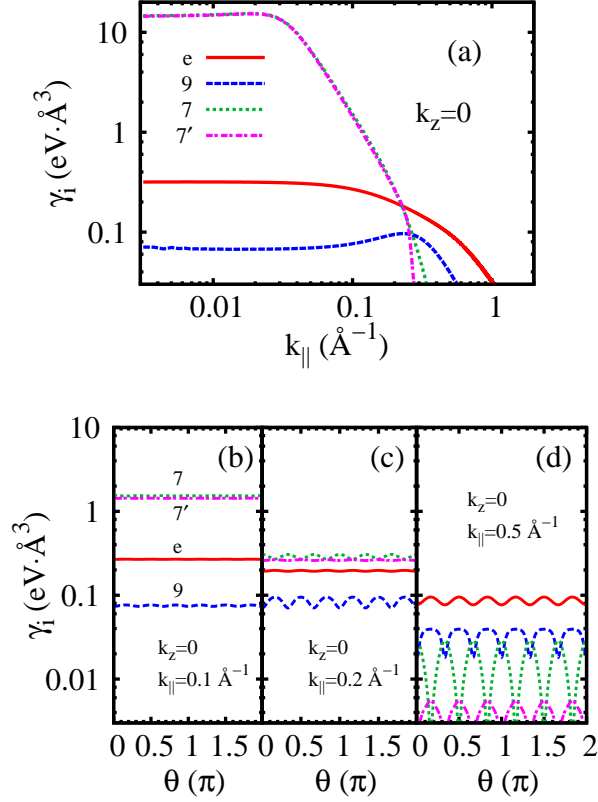


FIG. 5: (Color Online) (a) The SOC coefficients γ_i with $i = e, 9, 7, 7'$ vs. $k_{||}$ along Γ -K direction with $k_z=0$; (b-d) γ_i vs. angle of the momentum in the plane of $k_z=0$ with $k_{||}=0.1 \text{ \AA}^{-1}$ (b), $k_{||}=0.2 \text{ \AA}^{-1}$ (c), and $k_{||}=0.5 \text{ \AA}^{-1}$ (d).

the Γ point and is independent on the direction of the in-plane momentum. Here we obtain $\gamma_e \sim 0.51 \text{ eV}\cdot\text{\AA}^3$, which is also nearly two orders of magnitude smaller than that in GaAs.⁴⁶ The big difference comes from the smaller band gap of GaAs. When $k_{||} > 0.03 \text{ \AA}^{-1}$, γ_e decreases drastically with the momentum, and its angle dependence also becomes very pronounced.

The corresponding hole SOC coefficients are shown in Fig. 6(d) and (e). Near the Γ point, we find γ_8 and γ_7 around 30 and 25 $\text{eV}\cdot\text{\AA}^3$, respectively. Additionally, γ_8 shows stronger angle dependence of the momentum than γ_7 .

IV. CONCLUSION

In conclusion, we have investigated the electron and hole SOC up to third order in wurtzite semiconductors. Due to the intrinsic structure inversion asymmetry in addition to the bulk inversion asymmetry in wurtzite structure, both the linear Rashba effect and cubic Dresselhaus effect exist. We find the relative signs of the Rashba and Dresselhaus terms are opposite for electrons but are the same for holes in both ZnO and GaN. For holes with

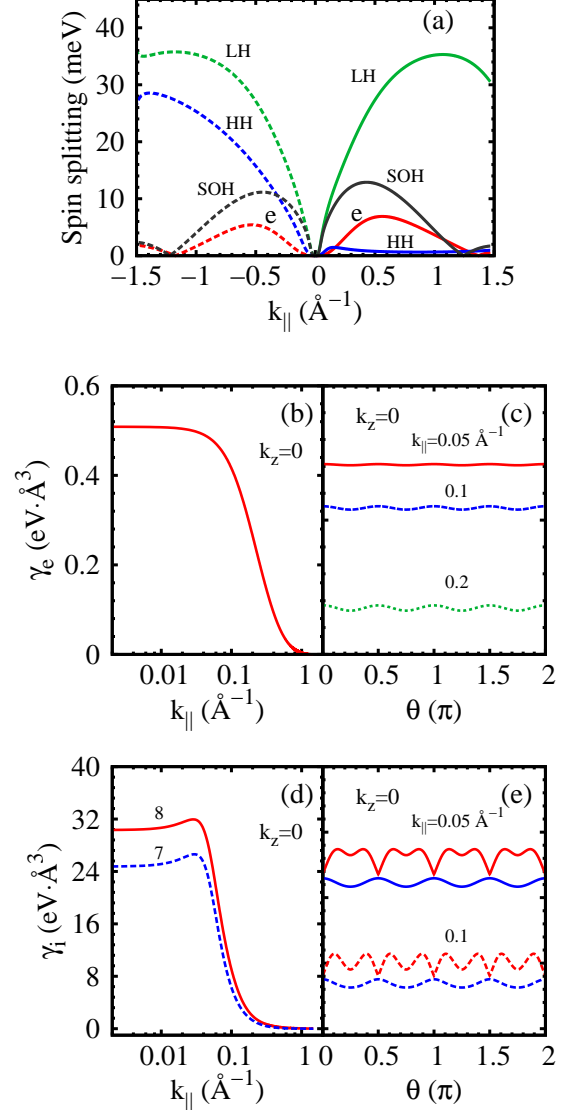


FIG. 6: (Color Online) (a) Electron and hole spin splitting in zinc-blende GaN against momentum along Γ -K (solid curves) and Γ -W (dashed curves) directions. Red curves: electron; Blue curves: HH; Green curves: LH; Black curves: SOH. (b) The corresponding electron SOC coefficient γ_e vs. $k_{||}$ along Γ -K direction. (c) γ_e vs. the angle of the momentum at different $k_{||}$ ($k_z = 0$). (d) γ_8 (red curve) and γ_7 (blue curve) vs. momentum along Γ -K direction with $k_z = 0$. (e) γ_8 (red curve) and γ_7 (blue curve) vs. the angle of the momentum at different $k_{||}$. Solid curves: $k_{||}=0.05$; Dashed curves: $k_{||}=0.1 \text{ \AA}^{-1}$.

Γ_{9v} symmetry, there is no linear Rashba contribution. Due to the negative spin splitting in ZnO, the signs of the Rashba coefficients for both electrons and holes are opposite with those in GaN.

The Dresselhaus spin splittings in wurtzite ZnO and GaN are calculated by the nearest-neighbor sp^3 TB model. We find that the electron Dresselhaus term becomes the dominant SOC compared with the linear

Rashba term when the electron concentration is higher than 10^{19} cm^{-3} for ZnO and 10^{20} cm^{-3} for GaN. While for the Γ_{7v} and $\Gamma_{7'v}$ holes, the linear term can not be neglected due to the relatively larger hole Rashba SOC coefficient. The corresponding SOC coefficients γ_i are also calculated, which are momentum-independent very near the Γ point. However, at large momentum, they decrease drastically and show strong angular dependence of the in-plane momentum. In addition, we confirm that the Dresselhaus parameter b is almost a constant for very small momentum and can be regarded approximately as an universal value for all the wurtzite materials as predicted in Ref. 25. However, for larger momentum, its k -dependence can not be neglected and the value varies strongly for different materials.

In order to compare with the zinc-blende structure, the spin splittings in cubic GaN are also addressed, calculated using sp^3s^* model. The isotropic spin splitting near the Γ point in wurzite structures does not hold in zinc-blende structure.

We believe that our results are useful for the on-going study of spin dynamics of ZnO and GaN. After all, due to

the small SOC in these wide gap semiconductors, the spin relaxation time becomes very long and hence more potential applications may be figured out using these semiconductors. Finally, we point out that due to the lack of the TB parameters for ZnO of zinc-blende structure, we cannot calculate the SOC coefficients for this structure. More investigations are needed.

Acknowledgments

This work was supported by the Natural Science Foundation of China under Grants No. 10574120 and No. 10725417, the National Basic Research Program of China under Grant No. 2006CB922005, the Knowledge Innovation Project of Chinese Academy of Sciences, and the Robert-Bosch Stiftung. One of the authors (M.W.W.) would like to thank X. Marie and U. Schwarz for bringing this topic into his attention as well as valuable discussions. J.Y.F. was also partially supported by China Postdoctoral Science Foundation.

-
- * Author to whom correspondence should be addressed; Electronic address: mwwu@ustc.edu.cn.
- ¹ D. M. Bagnall, Y. F. Chen, Z. Zhu, T. Yao, S. Koyama, M. Y. Shen, and T. Goto, Appl. Phys. Lett. **70**, 2230 (1997).
 - ² S. C. Jain, M. Willander, J. Narayan, and R. Van Overstraeten, J. Appl. Phys. **87**, 965 (2000).
 - ³ I. Vurgaftman and J. R. Meyer, J. Appl. Phys. **94**, 3675 (2003).
 - ⁴ A. Ashrafi and C. Jagadish, J. Appl. Phys. **102**, 071101 (2007); C. Klingshirn, phys. stat. sol. (b) **244**, 3027 (2007).
 - ⁵ K. S. Cho, Y. F. Chen, Y. Q. Tang, and B. Shen, Appl. Phys. Lett. **90**, 041909 (2007).
 - ⁶ X. W. He, B. Shen, Y. Q. Tang, N. Tang, C. M. Yin, F. J. Xu, Z. J. Yang, G. Y. Zhang, Y. H. Chen, C. G. Tang, and Z. G. Wang, Appl. Phys. Lett. **91**, 071912 (2007).
 - ⁷ S. S. Yan, C. Ren, X. Wang, Y. Xin, Z. X. Zhou, L. M. Mei, M. J. Ren, Y. X. Chen, Y. H. Liu, and H. Garmestani, Appl. Phys. Lett. **84**, 2376 (2004).
 - ⁸ S. Ghosh, V. Sih, W. H. Lau, D. D. Awschalom, S.-Y. Bae, S. Wang, S. Vaidya, and G. Chapline, Appl. Phys. Lett. **86**, 232507 (2005).
 - ⁹ W. K. Liu, K. M. Whitaker, A. L. Smith, K. R. Kittilstved, B. H. Robinson, and D. R. Gamelin, Phys. Rev. Lett. **98**, 186804 (2007).
 - ¹⁰ T. Dietl, H. Ohno, F. Matsukura, J. Cibert, and D. Ferrand, Science **287**, 1019 (2000).
 - ¹¹ B. Beschoten, E. Johnston-Halperin, D. K. Young, M. Poggio, J. E. Grimaldi, S. Keller, S. P. DenBaars, U. K. Mishra, E. L. Hu, and D. D. Awschalom, Phys. Rev. B **63**, 121202(R) (2001).
 - ¹² D. Lagarde, A. Balocchi, P. Renucci, H. Carrère, F. Zhao, T. Amand, X. Marie, Z. X. Mei, X. L. Du, and Q. K. Xue, arXiv:0804.2369.
 - ¹³ S. A. Wolf, J. Supercond. **13**, 195 (2000).
 - ¹⁴ I. Žutić, J. Fabian, S. D. Sarma, Rev. Mod. Phys. **76**, 323 (2004); J. Fabian, A. Matos-Abiad, C. Ertler, P. Stano, and I. Žutić, Acta Physica Slovaca **57**, 565 (2007).
 - ¹⁵ G. L. Bir and G. E. Pikus, *Symmetry and Strain-Induced Effects in Semiconductors* (Wiley, New York, 1974).
 - ¹⁶ W. Weber, S. D. Ganichev, S. N. Danilov, D. Weiss, W. Prettl, Z. D. Kvon, V. V. Bel'kov, L. E. Golub, Hyun-lck Cho, and Jung-Hee Lee, Appl. Phys. Lett. **87**, 262106 (2005).
 - ¹⁷ E. I. Rashba, Fiz. Tverd. Tela (Leningrad) **2**, 1224 (1960) [Sov. Phys. Solid State **2**, 1190 (1960)].
 - ¹⁸ Y. A. Bychkov and E. I. Rashba, Pis'ma Zh. Eksp. Teor. Fiz. **39**, 66 (1984) [Sov. Phys. JETP Lett. **39**, 78 (1984)].
 - ¹⁹ L. C. Lew Yan Voon, M. Willatzen, and M. Cardona, N. E. Christensen, Phys. Rev. B **53**, 10703 (1996).
 - ²⁰ J. A. Majewski and P. Vogl, *Physics of Semiconductors: 27th International Conference on the Physics of Semiconductors*, edited by J. Menéndez and C. G. Van de Walle (American Institute of Physics, 2005), p.1403.
 - ²¹ C. Kurdak, N. Biyikli, Ü. Özgür, H. Morkoc and V. I. Litvinov, Phys. Rev. B **74**, 113308 (2006).
 - ²² N. Thillozen, Th. Schäpers, N. Kaluza, H. Hardtdegen, and V. A. Guzenko, Appl. Phys. Lett. **88**, 022111 (2006).
 - ²³ S. Schmult, M. J. Manfra, A. Punnoose, A. M. Sergent, K. W. Baldwin, and R. J. Molnar, Phys. Rev. B **74**, 033302 (2006).
 - ²⁴ A. E. Belyaev, V. G. Raicheva, A. M. Kurakin, N. Klein, and S. A. Vitusevich, Phys. Rev. B **77**, 035311 (2008).
 - ²⁵ W. T. Wang, C. L. Wu, S. F. Tsay, M. H. Gau, I. Lo, H. F. Kao, D. J. Jang, J. C. Chiang, M. E. Lee, Y. C. Chang, C. N. Chen, and H. C. Hsueh, Appl. Phys. Lett. **91**, 082110 (2007).
 - ²⁶ P. Löwdin, J. Phys. Chem. **19**, 1396 (1951).
 - ²⁷ A. Kobayashi, O. F. Sankey, S. M. Volz, and J. D. Dow, Phys. Rev. B **28**, 935 (1983).
 - ²⁸ D. J. Chadi, Phys. Rev. B **16**, 790 (1977).

- ²⁹ S. L. Chuang and C. S. Chang, Phys. Rev. B **54**, 2491 (1996).
- ³⁰ E. Q. Kane, J. Phys. Chem. Solids **1**, 249 (1957).
- ³¹ R. Winkler, *Spin-Orbit Coupling Effects in Two-Dimensional Electron and Hole Systems* (Springer, Berlin, 2003).
- ³² D. J. Dugdale, S. Brand, and R. A. Abram, Phys. Rev. B **61**, 12933 (2000).
- ³³ I. Lo, W. T. Wang, M. H. Gau, S. F. Tsay, and J. C. Chiang, Phys. Rev. B **72**, 245329 (2005).
- ³⁴ P. Pfeffer and W. Zawadzki, Phys. Rev. B **72**, 035325 (2005).
- ³⁵ S. H. Wei and A. Zunger, Appl. Phys. Lett. **69**, 2719 (1996).
- ³⁶ M. Kumagai, S. L. Chuang, and H. Ando, Phys. Rev. B **57**, 15303 (1998).
- ³⁷ W. J. Fan, J. B. Xia, P. A. Agus, S. T. Tan, S. F. Yu, and X. W. Sun, J. Appl. Phys. **99**, 013702 (2006).
- ³⁸ J. E. Rowe, M. Cardona, and F. H. Pollak, Solid State Commun. **6**, 239 (1968).
- ³⁹ R. C. Casella, Phys. Rev. Lett. **5**, 371 (1960).
- ⁴⁰ G. D. Mahan and J. J. Hopfield, Phys. Rev. **135**, A428 (1964).
- ⁴¹ D. W. Jenkins and J. D. Dow, Phys. Rev. B **39**, 3317 (1989).
- ⁴² N. Malkova and C. Z. Ning, Phys. Rev. B **75**, 155407 (2007).
- ⁴³ K. Shindo, A. Morita, and H. Kamimura, J. Phys. Soc. Jap. **20**, 2054 (1965).
- ⁴⁴ J. C. Phillips, *Bonds and Bands in Semiconductors*, (Academic, San Diego, CA, 1973).
- ⁴⁵ N. Izyumskaya, V. Avrutin, Ü. Özgür, Y. I. Alivov, and H. Morkoc, phys. stat. sol. (b) **244**, 1439 (2007).
- ⁴⁶ J. Y. Fu, M. Q. Weng, and M. W. Wu, Physica E **40**, 2890 (2008).
- ⁴⁷ H. Morkoc, *Nitride Semiconductors and Devices* (2nd ed., Springer, Berlin, 2007).
- ⁴⁸ H. P. Maruska and J. J. Tietjen, Appl. Phys. Lett. **15**, 327 (1969).
- ⁴⁹ E. P. O'Reilly, A. Lindsay, S. Tomić, and M. K. Saadi, Semicond. Sci. Technol. **17**, 870 (2002).